J Mol Model (2015) 21: 245
DOI 10.1007/s00894-015-2790-2

ORIGINAL PAPER

Theoretical insights into the structures and mechanical properties of HMX/NQ cocrystal explosives and their complexes, and the influence of molecular ratios on their bonding energies

Yong-xiang Li[1,2] · **Shu-sen Chen**[1] · **Fu-de Ren**[2]

Received: 20 May 2015 / Accepted: 12 August 2015 / Published online: 29 August 2015

Abstract Molecular dynamics (MD) methods were employed to study the binding energies and mechanical properties of selected crystal planes of 1,3,5,7-tetranitro-1,3,5,7-tetrazacyclooctane (HMX)/nitroguanidine (NQ) cocrystals at different molecular molar ratios. The densities and detonation velocities of the cocrystals at different molar ratios were estimated. The intermolecular interaction and bond dissociation energy (BDE) of the N–NO_2 bond in the HMX:NQ (1:1) complex were calculated using the B3LYP, MP2(full) and M06-2X methods with the 6-311++G(d,p) and 6-311++G(2df,2p) basis sets. The results indicated that the HMX/NQ cocrystal prefers cocrystalizing in a 1:1 molar ratio, and the cocrystallization is dominated by the (0 2 0) and (1 0 0) facets. The *K*, *G*, and *E* values of the ratio of 1:1 are smaller than those of the other ratios, and the 1:1 cocrystal has the best ductility. The N–NO_2 bond becomes stronger upon the formation of the intermolecular H-bonding interaction and the sensitivity of HMX decreases in the cocrystal. This sensitivity change in the HMX/NQ cocrystal originates not only from the formation of the intermolecular interaction but also from the increment of the BDE of N–NO_2 bond in comparison with isolated HMX. The HMX/NQ (1:1) cocrystal exhibits good detonation performance. Reduced density gradient (RDG) reveals the nature of cocrystallization. Analysis of the surface electrostatic potential further confirmed that the sensitivity decreases in complex (or cocrystal) in comparison with that in isolated HMX.

Keywords HMX/NQ cocrystal · Molecular dynamics · Molecular ratios · Mechanical property · Bond dissociation energy · Intermolecular interaction · Electrostatic potential · RDG

Introduction

Energetic materials are used extensively for both military and civil purposes. However, most such materials do not meet the current requirements for insensitive high density energetic materials. The search for new insensitive and high energy explosives has been a primary goal in the field of energetic material chemistry in recent years [1, 2].

Cocrystals are a type of supramolecule, exhibiting intermolecular interactions arising from hydrogen bonds, π-stacking, van der Waals (vdW) forces, and electrostatic interactions, etc. [3–6]. The design of cocrystal explosives is one of the most promising approaches to decreasing sensitivity by favoring intermolecular interactions while maintaining the detonation performance of existing explosives [5, 7, 8]. Recently, much attention has been paid to the investigation of the synthesis, characterization and application of cocrystal explosives [9–14]. In theoretical studies, structural, electronic, and thermodynamic properties as well as intermolecular interactions of 1,3,5,7-tetranitro-1,3,5,7-tetrazacyclooctane (HMX)/1,3-dimethyl-2-imidazolidinone (DMI) cocrystal explosives were investigated using density functional theory (DFT). The calculated results were in reasonable agreement with experimental data [15, 16]. Ab initio and DFT were adopted to

Electronic supplementary material The online version of this article (doi:10.1007/s00894-015-2790-2) contains supplementary material, which is available to authorized users.

✉ Yong-xiang Li
liyongxiang101@126.com

[1] School of Materials Science and Engineering, Beijing Institute of Technology, Beijing 100081, China

[2] College of Chemical Engineering and Environment, North University of China, Taiyuan 030051, China

investigate the intermolecular H-bonds in HMX/5-nitro-1,2,4-triazol-3-one cocrystals [17]. Plots of the reduced density gradient (RDG) versus sign(λ_2)ρ were used to understand the internal mechanisms of 2,4,6-trinitrotoluene/2,4,6,8,10,12-hexanitrohexaazaisowurtzitane (CL-20) cocrystals [14].

It is well known that the stronger the intermolecular interactions, the more stable the cocrystal complex. Cocrystallization can be realized by combining two or more neutral components in a defined molecular molar ratio. The stability of a cocrystal can be affected by the ratio of the molecular combination because different molecular ratios have different intermolecular interaction energies. The ratio of molecular combination plays an important role in sensitivity and detonation performance of cocrystal explosives. In general, if a cocrystal explosive has too high a content of high energy explosive, the energy is enhanced and the sensitivity increases. However, high sensitivity is an undesirable property for an energetic material. On the contrary, if a cocrystal explosive has too high a content of low energy explosive with low sensitivity, the sensitivity decreases and simultaneously the energy will also be decreased. The latter is also an undesirable property. Thus, the content of high energy and low sensitivity explosive components must be controlled within a reasonable range. Therefore, it is very important for the design of cocrystals to determine the optimal ratio of molecular combination. In most of the published literature, only defined molecular ratios were reported. To our knowledge, few theoretical investigations on the influence of molecular ratios on the stabilities of cocrystal explosives have been presented.

HMX is a high energy and sensitive explosive. In order to reduce the sensitivity, cocrystal explosives involving HMX have been developed and are attracting increasing interest [15–23]. In 2009, Wei et al. [18] reported the theoretical calculation of cocrystal HMX/1,3,5-triamino-2,4,6-trinitro-benzene (TATB) using molecular dynamics (MD) simulation. In 2011, a cocrystal HMX/TATB explosive was prepared with a solvent/nonsolvent process and characterized by several experimental methods. The results indicated that the main properties of the cocrystal originate from the N–O···H hydrogen bonding between $–NO_2$ (HMX) and $–NH_2$ (TATB) [19, 20]. In 2012, the structures of seven cocrystals involving HMX were elucidated using single crystal X-ray diffraction, and drop-weight impact sensitivity was determined [21]. In 2013 and 2014, Lin et al. synthesized and characterized some cocrystal explosives involving HMX by using X-ray single crystal diffraction, including HMX/1,3-dimethyl-2-imidazolidinone [15], HMX/2,6-diamino-3,5-dinitropyrazine-1-oxide [22], HMX/5-nitro-1,2,4-triazol-3-one [17], and HMX/N-methyl-2-pyrrolidone [23].

Although its energy is not high in comparison with HMX, nitroguanidine (NQ) is an insensitive explosive [24]. The α-form of NQ comprises $–NH_2$, –NH– and $–NO_2$ groups, and HMX contains $–CH_2–$ and $–NO_2$ moieties. If HMX cocrystallizes with NQ, intermolecular H-bonds (N–H···O and C–H···O) can be formed, which stabilize the cocrystal. Furthermore, the sensitivity of HMX will decrease and the energy defect of NQ will be overcome. Thus, the HMX/NQ cocrystal represents a promising explosive for potentially widespread implementation in both military and civilian fields.

In this work, MD methods were employed to study the binding energies of selected crystal planes of the β-HMX/α-NQ cocrystal at different molecular molar ratios (β-HMX was selected because of its superior density and thermal stability). The mechanical properties of the cocrystal are also discussed. In order to obtain further information about bonding nature of the HMX/NQ cocrystal, the intermolecular interactions and bond dissociation energies (BDE) of the $N–NO_2$ bond in the 1:1 complex of HMX:NQ were calculated by ab initio and DFT methods, and RDG analysis was also carried out. Density and detonation velocity of the cocrystals at different molecular molar ratios were estimated. Molecular surface electrostatic potentials were used to judge the change in sensitivity upon complex formation. These studies will provide some novel insights that will inform the design of HMX cocrystal explosives.

Computational details

Molecular dynamics calculations

The unit cell model of HMX was constructed according to its cell parameters [25, 26]. The initial model was relaxed (COMPASS force-field, Smart algorithm) to produce a stable conformation using the Discover module (see Table S1). An accuracy of 1.0×10^{-5} kcal mol^{-1} was required to determine minimization convergence. The crystal morphologies of HMX in vacuum were predicted by the Growth morphology model. The major growth faces of HMX with relative attachment energies [E_{att} (Total), E_{att} (vdW), E_{att} (Elect), %A] are listed in Table S2. There are five major growth faces for HMX: (011), (11–1), (020), (10–2) and (100), in agreement with a previous investigation [27]. These growth faces suggest an important approach towards substituting to build cocrystal models. Therefore, in this paper, these five growth faces and an additional random face were selected to study the binding energies of HMX/NQ cocrystal in different molecular molar ratios in order to evaluate the influence of molecular ratio on stability of the cocrystal.

The HMX supercells were substituted by equal numbers of NQ moieties at 10:1, 9:1, 8:1, 7:1, 6:1, 5:1, 4:1, 3:1, 2:1 and 1:1 molar ratio (HMX:NQ). The selected parameters (molar ratios, mass ratios, supercell patterns and the number of substituted molecules) are listed in Table 1.

Table 1 Molecular molar ratios, mass ratios, super cell patterns and the numbers of substituted molecule in 1,3,5,7-tetranitro-1,3,5,7-tetrazacyclooctane (HMX)/nitroguanidine (NQ) cocrystals

Molar ratio (HMX:NQ)	Mass ratio[a]	Supercell pattern	Total number of molecules	Number of substituted molecules
10:1	0.9661	11×2×2	176	16
9:1	0.9624	5×2×2	80	8
8:1	0.9579	3×3×2	72	8
7:1	0.9522	4×2×2	64	8
6:1	0.9447	7×2×2	112	16
5:1	0.9343	3×2×2	48	8
4:1	0.9193	5×2×2	80	16
3:1	0.8952	2×2×2	32	8
2:1	0.8506	3×2×2	48	16
1:1	0.7400	2×2×2	32	16

[a] Mass percent of HMX

After building and geometry optimization of the substituted models, NVT ensembles and a temperature of 298 K were employed. Andersen was set as the temperature control method. COMPASS force-field was assigned above all MD simulations, and summation methods for electrostatic and vdW were Ewald and atom-based, respectively. The accuracy for the Ewald method was 1.0×10^{-4} kcal mol^{-1}. Cutoff distance and buffer width for the atom-based method were 15.5 Å and 2.0 Å, respectively. A 1.0 f. time step was set for MD processes, and the total dynamic time was 100,000 fs. The whole system reached an ideal state when the fluctuation of temperature and energy tended to be smooth with alternation less than 10 %. All MD calculations were carried out using MS 7.0.

An energy correction formula was involved in computing the corrected binding energy (E_b*) in order to standardize (make uniform) the differences caused by diverse supercells with different molecular molar ratios.

$$E_b^* = E_b \cdot N_0/N_i$$

Where E_b denotes the non-corrected binding energy, N_i is the number of molecule for different super cell, and N_0 the number of molecules for a standard pattern (molar ratio in 1:1).

Quantum-chemical calculations

According to the literature [14–16], in order to obtain further information about the bonding nature of the HMX/NQ cocrystal, HMX/NQ complexes (1:1) were designed by considering assembly motifs of HMX complexes with NQ. About ten stable complexes were obtained at the HF/6-311G (d,p) level. In these complexes, HMX molecules have the chair–ring conformation. Five structures of complexes were then selected and re-optimized at the B3LYP/6-311++G(d,p) level. Local minima were checked without any imaginary frequencies. Intermolecular interaction energies were calculated using the B3LYP, MP2(full), and M06-2X methods with the 6-311++G(d,p) and 6-311++G(2df,2p) basis sets, with correction of basis set superposition error (BSSE) [28]. Plots of RDG versus sign(λ_2)ρ were carried out at the B3LYP/6-311++G (d,p) level. All the above calculations were performed with Gaussian 09 [29] and Multiwfn 3.3.5 [30].

The BDEs of the N–NO_2 bonds involving hydrogen bonds were calculated at the B3LYP/6-311++G(d,p), B3LYP/6-311++G(2df,2p), MP2(full)/6-311++G(2df,2p), and M06-2X/6-311++G(2df,2p) levels. BDE was defined as:

$$BDE = E_{(R\cdot)} + E_{(\cdot NO_2)} - E_{(RNO_2)} \quad \text{for HMX molecule}$$

and

$$BDE = E_{(R\cdot)} + E_{(\cdot NO_2\cdots\ NQ)} - E_{(RNO_2\cdots NQ)} \quad \text{for complex}$$

where R· indicates the radical.

Results and discussion

Molecular dynamics analysis

Based on the MD simulation of substituted models, the corrected binding energies, E_b*, were calculated and are summarized in Table 2. Values were in the range of −1850.26 to −1064.08 kJ mol^{-1} in the 1:1 molar ratio (total number of molecules = 32, see Table 1). In the HMX/FOX-7 cocrystal, the binding energies were between −975.79 and −560.09 kcal mol^{-1} (i.e., −4080.75 and −2342.30 kJ mol^{-1}) in the 1:1 molar ratio (total number of molecules = 72) [27]. Comparing the results of binding energies from the HMX/FOX-7 cocrystal with the data shown in Table 2, it can be seen that our calculations are reliable.

The binding energy E_b* is a indication of component interaction strength. It influences the structural stability of the cocrystal and thus provides a general evaluation for screening

Table 2 Corrected binding energy, E_b*, of the substituted models with different molecular molar ratios[a]

	(0 1 1)	(1 1–1)	(0 2 0)	(1 0–2)	(1 0 0)	Random
10:1	−272.86	−337.41	−504.85	−245.14	−589.82	−343.14
9:1	−286.44	−343.81	−520.94	−250.41	−620.89	−350.50
8:1	−304.03	−351.62	−564.83	−262.11	−673.14	−368.42
7:1	−335.85	−366.85	−707.84	−302.19	−780.12	−395.77
6:1	−413.58	−415.95	−817.78	−373.01	−879.98	−432.89
5:1	−496.01	−512.34	−938.86	−450.27	−994.86	−529.40
4:1	−577.62	−643.17	−1188.75	−566.32	−1172.58	−679.34
3:1	−703.80	−862.08	−1367.49	−786.36	−1356.57	−879.21
2:1	−932.42	−1101.43	−1549.73	−1024.92	−1545.76	−1190.65
1:1	−1064.08	−1314.30	−1850.26	−1245.55	−1788.02	−1369.74

[a] Binding energy (E_b, in kJ mol^{-1}) was calculated from the following formula: $E_b = E_{tot} - (nE_{HMX} + mE_{NQ})$, where E_{tot}, E_{HMX} or E_{NQ} is single point energy of HMX/NQ cocrystal or monomer; n and m are the number of HMX and NQ molecules in the cocrystal, respectively

for preferred substituted patterns and molecular ratios. From Table 2, each different substituted pattern at each of the ratios holds a different binding energy. At a ratio of 1:1, the binding energy E_b* of the substituted pattern (0 2 0) is stronger than that of (1 0 0). In the ratios of 2:1, 3:1 and 4:1, the binding energies of (0 2 0) are close to those of (1 0 0). At the remaining ratios, the binding energies E_b* of (0 2 0) are weaker than those of (1 0 0). For all ratios, the binding energies are in the same order: random > (1 1–1) > (1 0–2) > (0 1 1). The substituted patterns (0 2 0) and (1 0 0) possess higher binding energies than the other patterns and are thus the most stable; cocrystallization is dominated by the (0 2 0) and (1 0 0) facets.

As can also be seen from Table 2, the different ratios in each of the substituted patterns hold different binding energies. For all the substituted patterns, the binding energies E_b* are in the same order of 1:1 > 2:1 > 3:1 > 4:1 > 5:1 > 6:1 > 7:1 > 8:1 > 9:1 > 10:1. At the ratio of 1:1, all the substituted patterns possess the strongest binding energies and HMX/NQ cocrystal prefers cocrystalizing in a 1:1 molecular molar ratio, while those at a ratio of 10:1 have the poorest binding energies. Many previous experimental results have also shown that cocrystals at low ratios, such as 1:1 and 2:1, were more stable [31, 32]. For example, Lin et al. [15] synthesized a cocrystal composed of HMX and DMI at a 1:1 molar ratio. A HMX/NMP cocrystal explosive at a 1:1 molar ratio was prepared [23]. The cocrystal of a 2:1 molar ratio of CL-20 and HMX has been reported experimentally [8]. Furthermore, from 1:1 to 5:1, the binding energies decreased sharply, while from 6:1 to 10:1, they decreased gently, and from 8:1 and 10:1, the corresponding values changed only slightly. For instance, for the (0 2 0) substituted pattern, from 1:1 to 5:1, the binding energies ranged from −1850.26 to −938.86 kJ mol^{-1}. However, from 6:1 to 10:1, the binding energy decreased by 312.93 kJ mol^{-1}, and from 8:1 and 10:1, the decrement of the binding energy was only 59.98 kJ mol^{-1}.

Mechanical properties

The mechanical properties are an important performance indicator in the preparation and usage of energetic materials. From the statistical mechanics of elasticity [33], the material stress and strain tensor are denoted by σ and ε, respectively. Hooke's law is stated as follows:

$$\sigma_I = C_{Ij}\varepsilon_j.$$

In this equation, C_{ij} is the elastic coefficient, which can be used to describe the stress–strain behavior of an arbitrary material.

Hardness, tensile strength and fracture strength can be related to the elastic modulus [34]. Hardness and tensile strength denoting the resistance to plastic deformation are proportional to the shear modulus G. Fracture strength is proportional to the bulk modulus K. Tensile modulus E and Poisson's ratio γ can be obtained by K and G with the equation $E = 2G(1 + \gamma) = 3K(1 - 2\gamma)$. The K/G and Cauchy pressure (C_{12}–C_{44}) can be taken as a criterion with which to evaluate the ductility or brittleness.

On the basis of MD simulations and the elastic static method, the mechanical properties of HMX/NQ co-crystals were estimated using the "constant strain" approach [35]. Table 3 presents the effective isotropic mechanical properties (K, G, C_{12}–C_{44}, γ, E and K/G) at different molecular ratios.

It can be seen from the values of C_{12}–C_{44} that the ductility of the material differs depending on the different molecular ratios, and the C_{12}–C_{44} values are in the following order: 1:1 > 2:1 > 3:1 > 4:1 > 5:1 > 7:1 > 6:1 > 8:1 > 10:1 > 9:1 (see Table 3). This result indicates that the 1:1 model has the better ductility.

From Table 3, the K, G, E values of the anisotropic cocrystals are in the order 1:1 < 2:1 < 3:1 < 4:1 < 5:1 < 6:1 < 7:1 < 8:1 < 9:1 < 10:1. Except for 7:1 and 10:1, the order of the K, G, E values is in accordance with that of the C_{12}–C_{44} values. The K, G, E values of the model with the 1:1 ratio are smaller than those of the other models, indicating that the rigidity of the model of 1:1 is the smallest. That is, to produce the same strain, less stress is required for the 1:1 model. Furthermore, the K/G value of model 1:1 is larger than that of models with other ratios, suggesting that the 1:1 model can hold the better ductility.

Therefore, the 1:1 cocrystal model can be inferred to have good mechanical properties. This model will deform more easily when subjected to an external force. Combined with the results of binding energy, one can see that the model with a molecular ratio of 1:1 will be more meaningful for experimental research.

Table 3 Mechanical properties of HMX/NQ cocrystal models at different molecular ratios[a]

	10:1	9:1	8:1	7:1	6:1	5:1	4:1	3:1	2:1	1:1
C_{12}–C_{44}	2.021	1.967	2.132	2.234	2.218	2.352	2.421	2.638	2.852	3.728
Poisson's ratio (γ)	0.263	0.266	0.268	0.275	0.283	0.290	0.297	0.301	0.307	0.351
Bulk modulus (K)	8.919	8.692	8.476	8.005	7.6082	7.106	6.752	6.127	5.682	4.023
Shear modulus (G)	5.021	4.820	4.652	4.238	3.860	3.470	3.170	2.812	2.517	1.331
tensile modulus (E)	12.683	12.204	11.799	10.807	9.906	8.954	8.224	7.316	6.580	3.597
K/G	1.776	1.803	1.822	1.889	1.971	2.048	2.130	2.180	2.257	3.022

[a] All modulus are in GPa

Structural analysis

To obtain further information about the bonding nature of the cocrystal, the structures of HMX/NQ (1:1) complexes were investigated (see Fig. 1). The intermolecular O···H and N···H distances were within 1.996 – 2.511 Å at the B3LYP/6-311++G (d, p) level, indicating that hydrogen bonds are formed between HMX and NQ. The C12–H13···N1 and N2–H3···O16 hydrogen bonds were confirmed in complex (A). Hydrogen bonds were also found in the other complexes: C12–H13···O7, N5–H6···O9 and N2–H4···O16 [as seen in (B)], N5–H6···O17 and N2–H4···O9 [as seen in ©)], C12–H13···O7, N5–H6···O17 and N2–H4···O9 [as seen in (D)], and C12–H13···O8 [as seen in (D)], respectively.

Interestingly, as shown in Fig. 1, the bond lengths of the N–NO_2 bonds involving hydrogen decrease in comparison with those in the isolated HMX molecule. This result is similar to the change in the C–NO_2 trigger-bond length upon formation of the intermolecular H-bonding interaction between the nitro group of CH_3NO_2 and HF [36]. Shortening of a bond length can lead to strengthening of that bond [37]. Thus, the N–NO_2 bond becomes stronger upon formation of the intermolecular H-bonding interaction. Both experimental and theoretical studies have verified that the trigger bond of HMX is N–NO_2 [38, 39]. In other words, the trigger bonds of N–NO_2 in the cocrystal complexes are more stable than those in the isolated HMX molecule. Thus, the sensitivity of HMX decreases in cocrystal explosives.

H-bonding interaction and BDE of the N–NO_2 bond

Table 4 lists the intermolecular H-bonding interaction energies calculated using the MP2(full) method, revealing that these are larger than those obtained with the B3LYP method. Interaction energies at the MP2(full)/6-311++G(2df,2p) level were close to those obtained at the M06-2X/6-311++G(2df,2p) level. At the MP2(full)/6-311++G(2df,2p) level, the intermolecular H-bonding interaction energies were within the range 24.3–39.2 kJ mol^{-1}. In our previous investigation into HF complexes with 1,2,4-triazoles, the H-bonding energies were in the range 20.6–27.7 kJ mol^{-1} at the same level [40]. In our study of the cocrystal complex CL-20/FOX-7, the intermolecular H-bonding energies were in the range 16.0–29.5 kJ mol^{-1} at the MP2(full)/6-311++G** level [41].

At four levels of theory, H-bonding interaction energies decrease in the same order of (A) ≈ (B) > ©) > (D) > (E). Hence, HMX/NQ cocrystals packed in complexes (A) and (B) are more stable.

The BDE of the trigger bond provides useful information with which to understand the stability of energetic materials [42, 43]. The BDE values calculated using the B3LYP method were all lower than those obtained by the MP2(full) and M06-2X methods (see Table 4). As mentioned in our previous work [36], the B3LYP method correctly describes the BDE values, but the MP2 method cannot be used to adequately describe BDEs [44, 45]. Therefore, the B3LYP/6-311++G(2df,2p) method was selected to elucidate trends in the calculated BDEs in this work. From Table 4, at the B3LYP/6-311++G(2df,2p) level, the order of the BDEs is (D) > ©) > (A) > (B) > (E).

The BDEs in the N–NO_2 bond in the complexes are larger than those in the isolated HMX. This result suggests that the strength of the N–NO_2 bond is enhanced upon formation of intermolecular H-bonds between HMX and NQ, which is in agreement with the structural analysis. The stronger the N–NO_2 trigger bond, the lower the sensitivity [46]. Thus, the explosive sensitivity decreases in complexes.

Therefore, we conclude that the HMX/NQ cocrystal explosive complex needs more energy not only to destroy the intermolecular H-bonding interactions, but also to counteract the increments of the BDEs of the N–NO_2 trigger-bonds in the process of detonation. This change in cocrystal explosive sensitivity originates not only from formation of the intermolecular H-bonding interaction but also from the increment of the N–NO_2 BDE. In previous investigations, the influence of the intermolecular H-bonding interaction on the strength of the N–NO_2 trigger-bond was not considered in cocrystal explosive complexes, with only the formation of intermolecular H-bonding interaction being regarded as the origin of the sensitivity change in cocrystal explosives [6, 17].

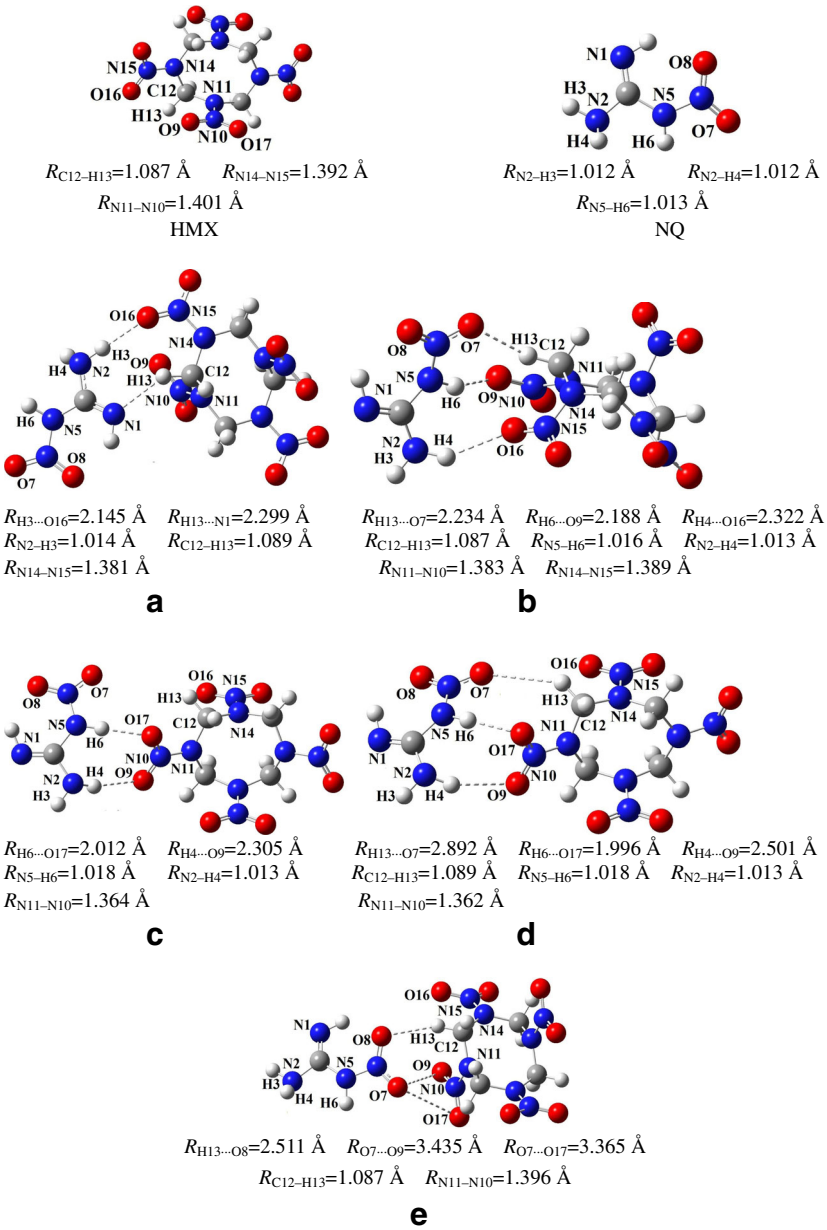

Fig. 1 Optimized structures and atomic numbers of 1,3,5,7-tetranitro-1,3,5,7-tetrazacyclooctane (HMX), nitroguanidine (NQ) and their complexes at the B3LYP/6-311++G (d, p) level

Table 4 Intermolecular hydrogen-bonding interaction energy [$-E_{int}$ (kJ mol^{-1})] and bond dissociation energy [BDE (kJ mol^{-1})] in the N–NO_2 bond [a]

	B3LYP/6-311++G(d,p)	B3LYP/6-311++G(2df,2p)	MP2(full)/6-311++G(2df,2p)	M06-2X/6-311++G(2df,2p)
(A)	33.6 (28.3) [192.3]	35.9 (30.5) [199.1]	39.2 (32.3) [239.5]	37.5 (31.6) [197.8]
(B)	32.6 (28.5) [185.5 180.8] [b]	35.7 (31.3) [187.9 186.5]	38.0 (33.6) [234.6 232.0]	38.9 (33.8) [192.3 191.6]
©)	29.0 (24.2) [203.5]	32.6 (28.2) [210.6]	33.1 (26.8) [255.6]	35.0 (27.3) [212.7]
(D)	27.3 (22.1) [218.8]	26.0 (23.0) [231.5]	29.8 (22.5) [272.8]	30.7 (24.6) [223.6]
(E)	20.6 (16.5) [175.6]	22.8 (19.1) [182.2]	24.3 (18.0) [203.5]	23.8 (17.8) [188.5]

[a] Values in parenthesis are basis set superposition error (BSSE)-corrected [$-E_{int.(BSSE)}$] hydrogen-bonding interaction energies. Values in square brackets are BDEs. The BDEs in the isolated HMX are 172.8, 179.0, 195.6 and 183.2 kJ mol^{-1} at the B3LYP/6-311++G(d,p), B3LYP/6-311++G(2df,2p), MP2(full)/6-311++G(2df,2p) and M06-2X/6-311++G(2df,2p) levels of theory, respectively

[b] BDE of the N11–N10 and N14–N15 bonds

RDG analysis

The RDG [47] can be used to reveal intermolecular and intramolecular interactions in real space based on the electron density. RDG is defined as

$$RDG = \frac{1}{2(3\pi^2)^{1/3}} \frac{|\nabla\rho(r)|}{\rho(r)^{4/3}}$$

According to Johnson et al. [47], the sign of λ_2 (the second eigenvalue of the electron density Hessian matrix) can be used to distinguish bonded ($\lambda_2 < 0$) from non-bonded ($\lambda_2 > 0$) interactions. In order to explore the features associated with small reduced gradients, plots of RDG versus sign [λ_2®)ρ(r)] were examined. Figure 2 depicts the RDG results of five complexes. The regions in low density and large reduced gradient correspond to the exponentially decaying tail regions of the density, i.e., far from the nuclei.

Most important for our present consideration were the regions of low density and low gradient. For the left-side region in each of complexes, several spikes lying at negative values were found in the low density and low gradient region (see upper panel in Fig. 3)—a signature of noncovalent interactions between HMX and NQ. The strong intramolecular interaction between the nitro-group and amine-group of NQ corresponds to the region of ~ −0.022 a.u. The intermolecular hydrogen-bonding interactions correspond to density values between −0.020 a.u. and −0.015 a.u. The moderate density values indicate that the intermolecular hydrogen-bonding interactions between nitro-groups of HMX and amine-groups of NQ are not strong, in agreement with the results of the molecular interaction energies. Density values between −0.015 a.u. and −0.005 a.u. (low reduced gradient) show vdW interactions.

The interaction regions can also be located by generating RDG isosurface enclosing the corresponding regions in real molecular space (lower panel in Fig. 3). The red isosurface corresponds to the repulsion and steric effect in the HMX ring or among chemical bonds. The blue and green isosurfaces between HMX and NQ correspond to the region in the low density, low-gradient spike lying at negative values, indicative of the attractive intermolecular interactions (i.e., intermolecular hydrogen-bonding interactions and vdW interactions). From Fig. 3, the weak H-bonds and vdW interactions are the main intermolecular interactions in HMX/NQ complexes. Note that, for complex (E), the blue isosurfaces are found in the region between the nitro-groups in HMX and NQ. This result shows that, in the complex (E), O···H and O···O interactions coexist. Indeed, according to natural bond orbital (NBO) analysis, the delocalization interaction $E^{(2)}_{\sigma(\mathrm{N10-O9})\rightarrow\mathrm{RY^*O7}}$ is up to 6.22 kJ mol^{-1} at the B3LYP/6-311++G (d, p) level.

Density and detonation velocity

Density (d_{mix}) and detonation velocity (V_{D}) are two important parameters for the cocrystallized systems of high density energetic materials. We calculated the theoretical mixing densities (d_{mix}) using the following equation [48]:

$$d_{\mathrm{mix}} = \Sigma m_I / \left(\Sigma m_I / d_{298\mathrm{K},I}\right)$$

where m_{I} is the mass of component I.

Since the heat of formation (HOF) of a solid cocrystal is the sum of its lattice energy and the HOF of the gaseous state of molecule, COMPASS field was employed to calculate lattice energy. According to Zhang et al. [48], the HOF of the gaseous state of molecule was derived from PM6 calculation. Then, the heats of detonation reactions were obtained by calculating HOF differences. Finally, V_{D} was evaluated using the Kamlet approximation [49].

All the results are given in Table 5. It was found that crystal density of cocrystal d_{mix} in each of ratios was slightly lower than that of HMX (i.e., the value at a ratio of 1:0), while higher than that of NQ (i.e., the value at a ratio of 0:1). The calculated detonation velocity of isolated HMX (1:0) or NQ (0:1) was larger slightly than the experimental result [49, 50]. The detonation velocity of HMX/NQ cocrystal at each of the ratios was slightly lower than that of HMX due to their low chemical energies, although larger than that of NQ. Although their detonation performance decreases slightly in contrast with HMX, they still exhibit good detonation performance. The d_{mix} (1.864 g cm^{-3}) and V_{D} (9.003 km s^{-1}) of HMX/NQ cocrystal in a 1:1 molecular molar ratio were very close to those of HMX. Therefore, HMX/NQ cocrystal in a 1:1 molar ratio is satisfactory in view of explosive properties.

Surface electrostatic potentials

Electrostatic potential (ESP) is a real and fundamentally significant physical property of compounds [52, 53]. Politzer et al. [46] suggested that, in addition to focusing on the trigger bond, the ESP, as a global feature of a molecule, should be taken into account in the analysis of explosive sensitivity. These latter authors found that the strongly positive central regions that characterize molecular surface potentials can be linked to sensitivity: the sensitivity increases as the central ESP becomes more positive. Furthermore, some quantitative relationships between the impact sensitivities and certain

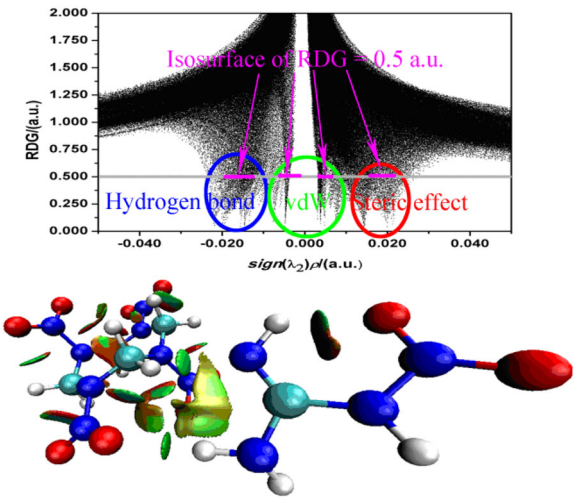
Isosurface of RDG = 0.5 a.u.
Hydrogen bond
vdW
Steric effect
RDG(a.u.)
sign(λ2)ρ(a.u.)

a

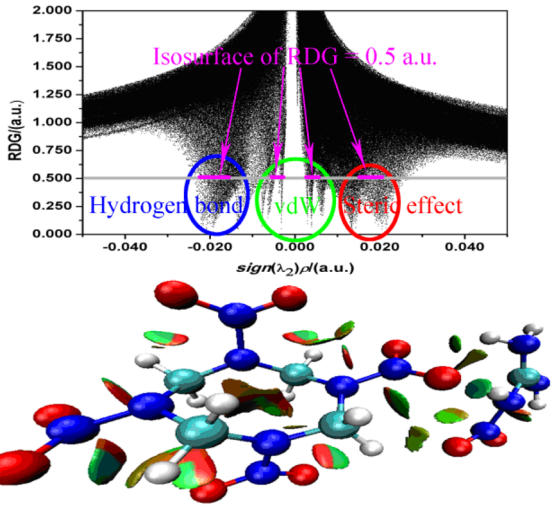
Isosurface of RDG = 0.5 a.u.
Hydrogen bond
vdW
Steric effect
RDG(a.u.)
sign(λ2)ρ(a.u.)

d

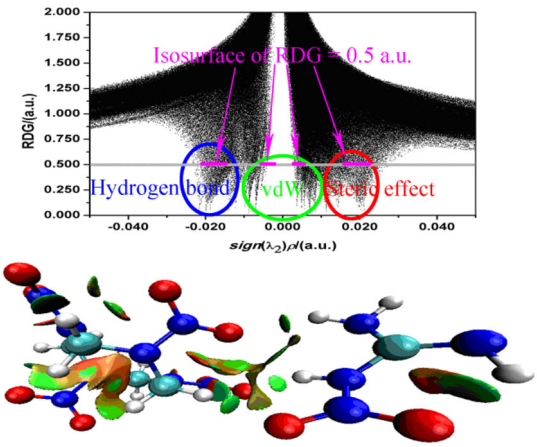
Isosurface of RDG = 0.5 a.u.
Hydrogen bond
vdW
Steric effect
RDG(a.u.)
sign(λ2)ρ(a.u.)

b

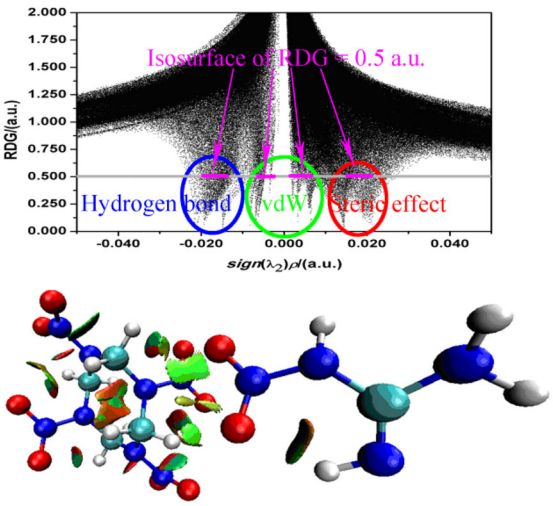
Isosurface of RDG = 0.5 a.u.
Hydrogen bond
vdW
Steric effect
RDG(a.u.)
sign(λ2)ρ(a.u.)

e

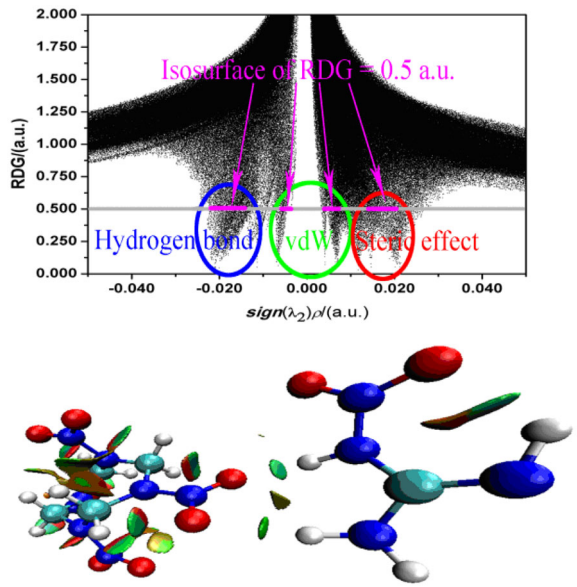
Isosurface of RDG = 0.5 a.u.
Hydrogen bond
vdW
Steric effect
RDG(a.u.)
sign(λ2)ρ(a.u.)

c

◀ **Fig. 2** *Upper panel* Plots of reduced density gradient (RDG) versus sign[λ2®)ρ®)], *lower panel* low-gradient (*s*=0.5 a.u.) isosurfaces for the HMX/NQ complex. The surfaces are colored on a *blue-green-red* scale according to values of sign(λ_2)ρ, ranging from –0.04 to 0.04 a.u. *Blue* Strong attractive H-bond, *green* van der Waals (vdW) interaction, *red* strong steric effect

features of the molecular surface ESPs, such as the positive variances of V_S®) (i.e., σ_+^2) and electrostatic balance parameter $\frac{\sigma_+^2\sigma_-^2}{(\sigma_+^2+\sigma_-^2)}$ ^{2}, have been established [54–60]. In 2013, Li et al. [14] used the ESP on the surface to evaluate the sensitivities of TNT and CL-20 both before and after co-crystal formation.

The ESP V_S(r) on the 0.001 a.u. molecular surfaces are shown in Figs. S1–S7 and Tables S3–S9. The surface minima ($V_{S,min}$) were associated mainly with the lone pairs of the O, N atoms in ring of HMX and N atoms in $–NH_2$ and –NH groups of NQ. The surface maxima ($V_{S,max}$) were located mainly near the H atom or the N atom of the $-NO_2$ group (see Figs. S1–S7 and Tables S3–S9). For all complexes, the largest value of $V_{S,max}$ was larger than that in the corresponding monomer.

Particularly interesting for us was the local maximum above the N−NO_2 bond involving intermolecular H-bonds. For the isolated molecules, such local $V_{S,max}$ have been found above the C−NO_2 or N−NO_2 bonds in nitroaromatics, nitroheterocycles, nitroalkanes or dimethylnitramine by Politzer and colleagues. Furthermore, these latter authors have stated that these $V_{S,max}$ values correlate inversely, to some extent, with C−NO_2 and N−NO_2 bond energies, and have been linked to impact sensitivities: the bond becomes weaker, i.e., the sensitivity becomes higher, as $V_{s,max}$ (C/N−NO_2) becomes more positive [58, 61–63]. From Figs. S1–S7 and Tables S3–S9, in ©), the $V_{S,max}$ above the N−NO_2 bond involving the intermolecular H-bonds was submerged by the strongly positive potential of hydrogens and the N atoms of the $-NO_2$ groups. However, the $V_{S,max}$ above the N−NO_2 bonds in HMX and NQ were found to be 25.58 and 27.15 kcal mol^{-1}, respectively, and those involving the H-bonds were 24.82, 19.61, 25.70 and 31.30 kcal mol^{-1} in (A), (B), (D) and (E), respectively. The $V_{S,max}$ above the N−NO_2 bonds in (A) and (B) were less positive than that in the isolated HMX, suggesting that the N−NO_2 bonds become

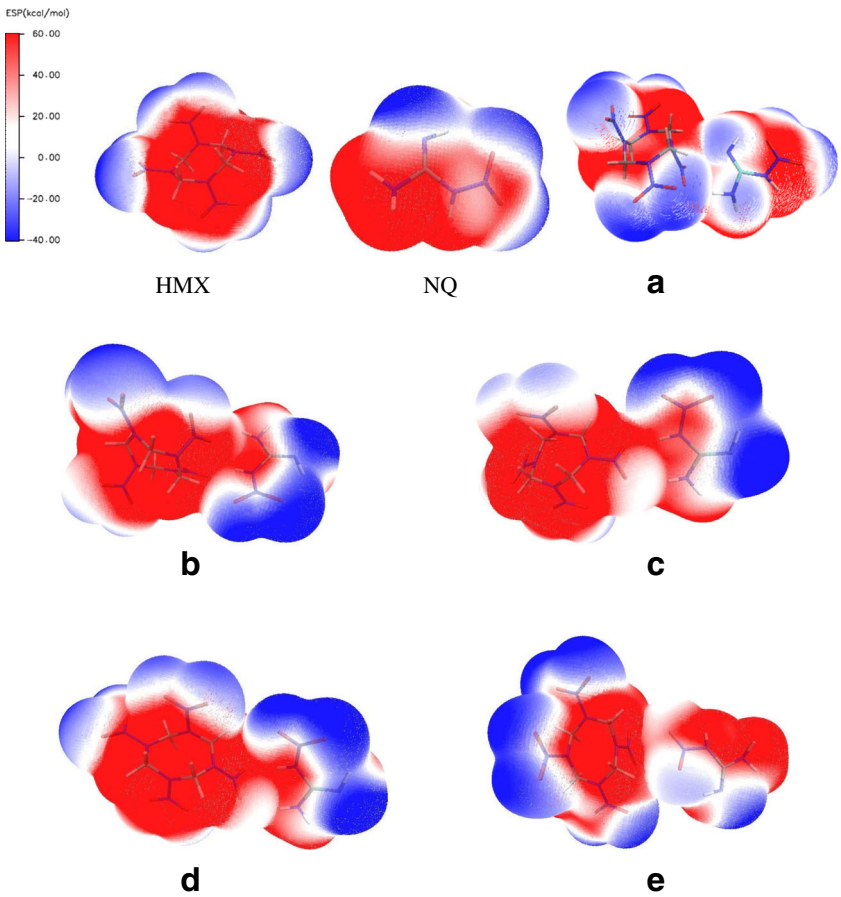

Fig. 3 Electrostatic potential surface of HMX, NQ and their complexes

Table 5 Predicted properties [d_{mix} (g cm^{-3}) and V_D(km s^{-1})] at different molecular molar ratios (HMX:NQ)

	1:0	10:1	9:1	8:1	7:1	6:1	5:1	4:1	3:1	2:1	1:1	0:1
d_{mix}	1.905 [a]	1.899	1.899	1.898	1.897	1.896	1.894	1.892	1.888	1.881	1.864	1.755 [b]
V_D	9.14[c] 9.312	9.209	9.203	9.195	9.186	9.175	9.162	9.144	9.123	9.097	9.003	7.739[d] 8.252

[a] Data from [26]

[b] Data from [50]

[b] Calculated data from [48]

[d] Experimental data cited from [51]

stronger and the sensitivity becomes lower upon complex formation, in accordance with results from the structure and BDEs of the N−NO_2 bonds.

The values of the positive and negative variances of V_S®) (i.e., σ_+^2 and σ_-^2), and the electrostatic balance parameter $\frac{\sigma_+^2\sigma_-^2}{(\sigma_+^2+\sigma_-^2)}$ ^{2} (ν) are collected in Table 6. $\sigma_+^2 > \sigma_-^2$ is found in HMX, NQ and their complexes, in accordance with the features of energetic explosives with strong NO_2 electron-attracting groups [58].

From the relationship between the impact sensitivities and the features of surface ESPs (σ_+^2 and ν) [64], the smaller the value of σ_+^2, the larger the value of ν, and, simultaneously, the lower the impact sensitivity becomes. From Table 6, for complexes (A) and (E), the values of σ_+^2 [196.88 and 197.74 (kcal mol^{-1})^2] were smaller than that of isolated HMX [206.20 (kcal mol^{-1})^2], and, simultaneously, the values of ν (0.1430 and 0.1763) were larger than that of isolated HMX (0.1350). Thus, the impact sensitivities of (A) and (E) decrease in comparison with that in isolated HMX. However, for complexes (B), ©) and (D), although the values of ν were larger than that of isolated HMX, the values of σ_+^2 were also larger than that of HMX. Thus, for these three complexes, we cannot judge whether the sensitivity decreases or increases in comparison with that in HMX. For complexes (B) and (D), the values of σ_+^2 were larger than that of isolated NQ, and, simultaneously, the values of ν were smaller than that of isolated NQ. Thus, the impact sensitivities of (B) and (D) increase in comparison with that in isolated NQ. In previous investigations, although for isolated molecules some relationships between the impact sensitivities and the features of surface ESPs (σ_+^2 and ν) were established, unfortunately they were not established for the intermolecular H-bonded complexes. Therefore, the quantitative impact sensitivities h_{50} were not calculated in this work.

It is worth mentioning that, although for (B), ©) and (D), we cannot judge whether the sensitivity decreases or increases, for the most stable complex (A), which dominates the cocrystallization, it has been confirmed that the sensitivity decreases in comparison with that in HMX. Therefore, it can be concluded that the sensitivity decreases in the cocrystal HMX/NQ in comparison with that in isolated HMX.

Conclusions

In this paper, MD methods were employed to study the binding energies and mechanical properties of selected crystal planes for the HMX/NQ cocrystal at different molecular molar ratios. Density and detonation velocity of the cocrystals at different molecular molar ratios were estimated. The intermolecular interactions and BDE of N–NO_2 bond in the 1:1 complex of HMX:NQ were calculated. The results indicate that HMX/NQ cocrystal prefers cocrystalizing in a 1:1 molecular molar ratio, and the cocrystallization is dominated by the (0 2 0) and (1 0 0) facets. The *K*, *G*, *E* values of the model of 1:1 were smaller than those of the other models and the 1:1 cocrystal has the best ductility. The N–NO_2 bond becomes stronger upon formation of the intermolecular H-bonding interaction, and the sensitivity of HMX decreases in the cocrystal. The change in cocrystal explosive sensitivity originates not only from the formation of the intermolecular interaction but also from the increment of the N–NO_2 BDE. HMX/NQ (1:1) cocrystals exhibit good detonation performance. The surface electrostatic potential analysis further confirms that the sensitivity decreases in complex (or cocrystal) in comparison with that in isolated HMX. These studies

Table 6 Computed molecular surface potentials σ_+^2 and σ_-^2 [in (kcal mol^{-1})^2], and electrostatic balance parameter $\frac{\sigma_+^2\sigma_-^2}{(\sigma_+^2+\sigma_-^2)}$ ^{2} (ν)

	HMX	NQ	(A)	(B)	©)	(D)	(E)
σ_+^2	206.20	202.98	196.88	220.99	259.22	249.15	197.74
σ_-^2	39.52	65.51	41.16	64.91	86.01	65.82	58.59
ν	0.1350	0.1845	0.1430	0.1755	0.1871	0.1653	0.1763

provide some novel insights that will aid the design of HMX cocrystal explosives.

Ethical statement We have full control of all primary data and agree to allow the journal to review all the data if requested. We confirm the validity of the results from this manuscript. We have no financial relationships to declare. The manuscript has not been submitted to more than one journal, and it has not been published previously. This study is not split up into several parts to increase the quantity of submissions and submitted to various journals or to one journal over time. No data have been fabricated or manipulated.

Appendix A

Cell parameters and main stable surfaces of HMX in vacuum as well as the surface electrostatic potentials are in Appendix A.

References

1. Landenberger KB, Bolton O, Matzger AJ (2013) Two isostructural explosive cocrystals with significantly different thermodynamic stabilities. Angew Chem Int Ed 52:6468–6471
2. Thottempudi V, Shreeve JM (2011) Synthesis and promising properties of a new family of high-density energetic salts of 5-Nitro-3-trinitromethyl-1H-1, 2,4-triazole and 5,5'-Bis(trinitromethyl)-3,3'-azo-1H-1,2,4-triazole. J Am Chem Soc 133:19982–19992
3. Lindoy LF, Atkinson IM (2000) Self-assembly in supramolecular systems. Royal Society of Chemistry, London
4. Lehn JM (1988) Supramolecular chemistry-scope and perspectives molecules, supermolecules, and molecular devices (Nobel Lecture). Angew Chem Int Ed 27:89–112
5. Lara-Ochoa F, Espinosa-Pérez G (2007) Cocrystals definitions. Supramol Chem 19:553–557
6. Zhang H, Guo C, Wang X, Xu J, He X, Liu Y, Liu X, Huang H, Sun J (2013) Five energetic cocrystals of BTF by intermolecular hydrogen bond and π-stacking interactions. Cryst Growth Des 13:679–687
7. Bolton O, Matzger AJ (2011) Improved stability and smart-material functionality realized in an energetic cocrystal. Angew Chem Int Ed 50:8960–8963
8. Bolton O, Simke LR, Pagoria PF, Matzger AJ (2012) High power explosive with good sensitivity: A 2:1 cocrystal of CL-20:HMX. Cryst Growth Des 12:4311–4314
9. Guo C, Zhang H, Wang X, Xua J, Liu Y, Liu X, Huang H, Sun J (2013) Crystal structure and explosive performance of a new CL-20/caprolactam cocrystal. J Mol Struct 1048:267–273
10. Wang Y, Yang Z, Li H, Zhou X, Zhang Q, Wang J, Liu Y (2014) A novel cocrystal explosive of HNIW with good comprehensive properties. Propellants Explos Pyrotech 39(4):590–596
11. Yang Z, Li H, Zhou X, Zhang C, Huang H, Li J, Nie F (2012) Characterization and properties of a novel energetic-energetic cocrystal explosive composed of HNIW and BTF. Cryst Growth Des 12:5155–5158
12. Evers J, Gospodinov I, Joas M, Klapötke TM, Stierstorfer J (2014) Cocrystallization of photosensitive energetic copper(II) perchlorate complexes with the nitrogen-rich ligand 1,2-di(1H-tetrazol-5-yl)ethane. Inorg Chem 53:11749–11756
13. Millar DIA, Maynard-Casely HE, Allan DR, Cumming AS, Lennie AR, Mackay AJ, Oswald IDH, Tang CC, Pulham CR (2012) Crystal engineering of energetic materials: co-crystals of CL-20. CrystEngComm 14:3742–3749
14. Li H, Shu Y, Gao S, Chen L, Ma Q, Ju X (2013) Easy methods to study the smart energetic TNT/CL-20 co-crystal. J Mol Model 19: 4909–4917
15. Lin H, Zhu SG, Li HZ, Peng XH (2013) Synthesis, characterization, AIM and NBO analysis of HMX/DMI cocrystal explosive. J Mol Struct 1048:339–348
16. Gu B, Lin H, Zhu S (2014) Ab initio studies of 1,3,5,7-tetranitro-1, 3,5,7-tetrazocine/ 1,3-dimethyl-2-imidazolidinone cocrystal under high pressure using dispersion corrected density functional theory. J Appl Phys 115:143509-1–143509-8
17. Lin H, Zhu S, Zhang L, Peng X, Chen P, Li H (2013) Intermolecular interactions, thermodynamic properties, crystal structure, and detonation performance of HMX/NTO cocrystal explosive. Int J Quantum Chem 113:1591–1599
18. Wei C, Duan X, Liu C, Liu Y, Li J (2009) Molecular simulation on co-crystal structure of HMX/TATB. Acta Chim Sin 67:2822–2826
19. Jin PS, Duan XH, Luo QP, Zhou Y, Bao Q, Ma YJ, Pei CH (2011) Preparation and characterization of a novel cocrystal explosive. Cryst Growth Des 11:1759–1765
20. Wei C, Huang H, Duan X, Pei C (2011) Structures and properties prediction of HMX/TATB co-crystal. Propellants Explos Pyrotech 36:416–423
21. Landenberger KB, Matzger AJ (2012) Cocrystals of 1,3,5,7-Tetranitro-1,3,5,7-tetrazacyclooctane (HMX). Cryst Growth Des 12:3603–3609
22. Lin H, Zhu S, Li H, Peng X (2013) Structure and detonation performance of a novel HMX/LLM-105 cocrystal explosive. J Phys Org Chem 26:898–907
23. Lin H, Zhu SG, Zhang L, Peng XH, Li HZ (2014) Synthesis and first principles investigation of HMX/NMP cocrystal explosive. J Energ Mater 31:261–272
24. Astakhov AM, Dyugnev KP, Kuzubov AA, Nasluzov VA, Vasiliev AD, Buka ES (2009) Theoretical studies of the structure of nitrimines. I. structure of 2-nitroguanidine and its alkyl derivatives. J Struct Chem 50:201–211
25. Chang BC, Choi S, Boutin HP (1970) A study of the crystal structure of β-cyclotetramethylene tetranitramine by neutron diffraction. Acta Crystallogr B 26:1235–1240
26. Choi CS, Prince E (1972) The crystal structure of cyclotrimethylenetrinitramine. Acta Crystallogr B 28:2857–2862
27. Lin H, Zhang L, Zhu S, Li H, Peng X (2012) Molecular dynamic simulation of cyclotetramethylene tetranitramine/1,1-diamino-2,2-dinitroethylene co-crystal explosive. ACTA Armamentarii 33: 1025–1030
28. Boys SF, Bernardi F (1970) The calculation of small molecular interactions by the differences of separate total energies. Some procedures with reduced errors. Mol Phys 19:553–566
29. Frisch MJ, Trucks GW, Schlegel HB, Scuseria GE, Robb MA, Cheeseman JR, Scalmani G, Barone V, Mennucci B, Petersson GA, Nakatsuji H, Caricato M, Li X, Hratchian HP, Izmaylov AF, Bloino J, Zheng G, Sonnenberg JL, Hada M, Ehara M, Toyota K, Fukuda R, Hasegawa J, Ishida M, Nakajima T, Honda Y, Kitao O, Nakai H, Vreven T, Montgomery JA, Jr, Peralta JE, Ogliaro F, Bearpark M, Heyd JJ, Brothers E, Kudin KN, Staroverov VN, Kobayashi R, Normand J, Raghavachari K, Rendell A, Burant JC, Iyengar SS, Tomasi J, Cossi M, Rega N, Millam JM, Klene M, Knox JE, Cross JB, Bakken V, Adamo C, Jaramillo J, Gomperts R, Stratmann RE, Yazyev O, Austin AJ, Cammi R, Pomelli C, Ochterski JW, Martin RL, Morokuma K, Zakrzewski VG, Voth GA, Salvador P, Dannenberg JJ, Dapprich S, Daniels AD, Farkas O, Foresman JB, Ortiz JV, Cioslowski J, Fox DJ (2009) Gaussian 09, Inc.. USA, Wallingford CT

30. Lu T (2014) Multiwfn: a multifunctional wavefunction analyzer, Version 3.3.5. Beijing
31. Atzger AJ, Bolton O (2011) Improved stability and smart-material functionality realized in an energetic cocrystal. Angew Chem Int Ed 50:8960–8963
32. Landenberger KB, Matzger AJ (2010) Cocrystal engineering of a prototype energetic materials supramolecular chemistry of 2, 4, 6-trinitrotoluene. Cryst Growth Des 10:5341–5347
33. Weiner JH (1983) Statistical mechanics of elasticity. Wiley, New York
34. Pugh SF (1954) XCII. Relations between the elastic moduli and the plastic properties of polycrystalline pure metals. Philos Mag 45(367):823–843
35. Grimme S (2006) Semiempirical GGA-type density functional constructed with a long-range dispersion correction. J Comput Chem 27:1787–1799
36. Wang HB, Shi WJ, Ren FD, Yang L, Wang JL (2012) A B3LYP and MP2(full) theoretical investigation into explosive sensitivity upon the formation of the intermolecular hydrogen-bonding interaction between the nitro group of RNO_2 (R = $-CH_3$, $-NH_2$, $-OCH_3$) and HF, HCl or HBr. Comput Theor Chem 994:73–80
37. Macaveiu L, Göbel M, Klapötke TM, Murray JS, Politzer P (2010) The unique role of the nitro group in intramolecular interactions: chloronitromethanes. Struct Chem 21:139–146
38. Zhu W, Wang XJ, Xiao JJ, Zhu HW, Sun H, Xiao HM (2009) Molecular dynamics simulations of AP/HMX composite with a modified force field. J Hazard Mater 167:810–816
39. Brill BT, James K (1993) Kinetics and mechanisms of thermal decomposition of nitroaromatic explosive. Chem Rev 93:2667–2692
40. Li BH, Shi WJ, Ren FD, Wang Y (2013) A B3LYP and MP2(full) theoretical investigation into the strength of the C–NO_2 bond upon the formation of the intermolecular hydrogen-bonding interaction between HF and the nitro group of nitrotriazole or its methyl derivatives. J Mol Model 19:511–519
41. Gao HF, Zhang SH, Ren FD, Liu F, Gou RJ, Ding X (2015) Theoretical Insight into the Co-crystal Explosive of 2,4,6,8,10,12-hexanitrohexaazaisowurtzitane (CL-20)/1,1-diamino-2,2-dinitroethylene (FOX-7). Comput Mater Sci. doi:10.1016/j.commatsci.2015.05.009, **In Press**
42. Liu H, Wang F, Wang GX, Gong XD (2012) Theoretical studies of -NH_2 and -NO_2 substituted dipyridines. J Mol Model 18:4639–4647
43. Wu Q, Pan Y, Zhu WH, Xiao HM (2013) Computational study of energetic nitrogen-rich derivatives of 1,4-bis(1-azo-2,4-dinitrobenzene)-iminotetrazole. J Mol Model 19:1853–1864
44. Budyka MF, Zyubina TS, Zarkadis AK (2002) Correlating ground and excited state properties: a quantum chemical study of the photodissociation of the C–N bond in N-substituted anilines. J Mol Struct (THEOCHEM) 594:113–125
45. Brinck T, Haeberlin M, Jonsson M (1997) A computational analysis of substituent effects on the O−H bond dissociation energy in phenols: polar versus radical effects. J Am Chem Soc 119:4239–4244
46. Politzer P, Murray JS (2014) Impact sensitivity and crystal lattice compressibility/free space. J Mol Model 20:2223–2230
47. Johnson ER, Keinan S, Mori-Sánchez P, Contreras-Garcia J, Cohen AL, Yang W (2010) Revealing noncovalent interactions. J Am Chem Soc 132:6498–6506
48. Zhang C, Cao Y, Li H, Zhou Y, Zhou J, Gao T, Zhang H, Yang Z, Jiang G (2013) Toward low-sensitive and high-energetic cocrystal I: evaluation of the power and the safety of observed energetic cocrystals. Cryst Eng Commun 15:4003–4014
49. Kamlet MJ, Jacobs SJ (1968) Chemistry of detonations. I. A simple method for calculating detonation properties of C–H–N–O explosives. J Chem Phys 48:23–25
50. Bracuti AJ (1999) Crystal structure refinement of nitroguanidine. J Chem Crystallogr 29:671–676
51. Duan W, Lv Z (2003) Mechanical sensitivity and explosive performance of nitroguanidine (NQ)-based composite explosives. Chin J Energ Mater 11:209–212
52. Politzer P, Murray JS (2002) The fundamental nature and role of the electrostatic potential in atoms and molecules. Theor Chem Acc 108:134–142
53. Murray JS, Politzer P (2011) The electrostatic potential: an overview. WIREs Comput Mol Sci 1:153–163
54. Rice BM, Hare JJ (2002) A quantum mechanical investigation of the relation between impact sensitivity and the charge distribution in energetic molecules. J Phys Chem A 106:1770–1783
55. Murray JS, Concha MC, Politzer P (2009) Links between surface electrostatic potentials of energetic molecules, impact sensitivities and C–NO_2/N–NO_2 bond dissociation energies. Mol Phys 107:89–97
56. Politzer P, Murray JS (2014) In: Brinck T (ed) Green energetic materials. Chichester, Wiley, pp 45–62, **ch 3**
57. Politzer P, Murray JS (2014) Detonation performance and sensitivity: a quest for balance. Adv Quantum Chem 69:1–30
58. Politzer P, Murray JS (1996) Relationships between dissociation energies and electrostatic potentials of C–NO_2 bonds: applications to impact sensitivities. J Mol Struct 376:419–424
59. Murray JS, Lane P, Politzer P (1998) Effects of strongly electron-attracting components on molecular surface electrostatic potentials: application to predicting impact sensitivities of energetic molecules. Mol Phys 93:187–194
60. Politzer P, Murray JS (2015) Some molecular/crystalline factors that affect the sensitivities of energetic materials: molecular surface electrostatic potentials, lattice free space and maximum heat of detonation per unit volume. J Mol Model 21:25–35
61. Murray JS, Lane P, Politzer P (1995) Relationships between impact sensitivities and molecular surface electrostatic potentials of nitroaromatic and nitroheterocyclic molecules. Mol Phys 85:1–8
62. Politzer P, Murray JS (1995) C–NO_2 dissociation energies and surface electrostatic potential maxima in relation to the impact sensitivities of some nitroheterocyclic molecules. Mol Phys 86:251–255
63. Politzer P, Murray JS, Concha MC, Lane P (2007) Effects of electric fields upon energetic molecules: nitromethane and dimethylnitramine. Cent Eur J Energetic Mater 4:3–21
64. Pospíšil M, Vávra P, Concha MC, Murray JS, Politzer P (2010) A possible crystal volume factor in the impact sensitivities of some energetic compounds. J Mol Model 16:895–901